Article

Feasibility Study of Micro-Wind Turbines for Powering Wireless Sensors on a Cable-Stayed Bridge

Jong-Woong Park [1], Hyung-Jo Jung [1,*], Hongki Jo [2] and Billie F. Spencer, Jr. [2]

[1] Department of Civil and Environmental Engineering, Korea Advanced Institute of Science and Technology (KAIST), Daejeon 305-701, Korea; E-Mail: jwp@kaist.ac.kr

[2] Department of Civil and Environmental Engineering, University of Illinois at Urbana-Champaign, Urbana and Champaign, IL 61801, USA; E-Mails: hjo4@illinois.edu (H.J.); bfs@illinois.edu (B.F.S.)

* Author to whom correspondence should be addressed; E-Mail: hjung@kaist.ac.kr; Tel.: +82-42-350-3626; Fax: +82-42-350-3610.

Abstract: In this study, the feasibility of using micro-wind turbines to power wireless sensors on a cable-stayed bridge is comprehensively investigated. To this end, the wind environment around a bridge onto which a turbine is installed is examined, as is the power consumption of a wireless sensor. Feasible alternators and rotors are then carefully selected to make an effective small wind generator (known as a micro-wind turbine). Using the three specially selected micro-wind turbines, a series of experiments was conducted to find the turbine best able to generate the largest amount of power. Finally, a horizontal-axis micro-wind turbine with a six-blade rotor was combined with a wireless sensor to validate experimentally its actual power-charging capability. It is demonstrated that the micro-wind turbine can generate sufficient electricity to power a wireless sensor under moderate wind conditions.

1. Introduction

Due to their cost-effectiveness and ease of installation, the use of wireless sensors (WSs) for the structural health monitoring (SHM) of bridges has recently become an area of interest in the field of civil engineering. In one recent achievement, 70 wireless sensors were installed on the second Jindo Bridge in South Korea in 2009 to monitor the long-term structural behavior of the bridge [1,2]. Most of the sensor nodes were operated by high-capacity D-cell batteries, which are very heavy and large in comparison to the WSs. Moreover, the batteries need to be replaced at least every two months, not being able to last for more than this amount of time despite the use of an effective power-saving strategy known as *SnoozeAlarm* [2], which allows the sensor network to sleep most of the time. In order to realize a long-term SHM system based on wireless sensors, the power supply issue must be properly addressed.

The most promising solution to the abovementioned problem is to develop an efficient and reliable energy-harvesting device that extracts energy from the environment. There are several possible devices for energy harvesting, and the majority of them use energy from sunlight, vibrations or thermal gradients. Table 1 lists the energy-harvesting characteristics of several different technologies.

Table 1. Energy-harvesting characteristics [3].

Harvesting Technology	Condition	Power Density
Photovoltaic cells (Solar)	Outdoors	7500 μW/cm^2
Photovoltaic cells (Solar)	Indoors	100 μW/cm^2
Vibrations	1 m/s^2	100 μW/cm^3
Thermal gradients	$\Delta T = 5$ °C	60 μW/cm^2

As shown in the table, the power density of photovoltaic (PV) cells, often termed solar cells [4,5], is clearly greater than the densities of all of the other alternative technologies listed. However, charging batteries with solar panels is not always a pragmatic solution, as the energy source, *i.e.*, the Sun, does not emit sufficient light at all hours of the day. This is especially true in shaded areas. This limitation of solar panels was clearly validated in a field test of the long-term wireless sensors deployed on the second Jindo Bridge. Figure 1 shows the charging status of rechargeable batteries powered by solar panels in the test. As shown in the figure, the voltage levels of all of the batteries located on cables did not decline, whereas the voltage of the battery under the deck declined significantly with time, as the solar panels under the deck did not receive sufficient sunlight during the test. A wireless sensor placed under the deck may be stably operated by connecting to a solar panel positioned in a proper location, which is sometimes far away from the sensor, through a power line. However, this approach needs additional facilities and costs such as long power lines and wiring work, resulting in the loss of the most distinctive feature of a wireless sensor (*i.e.*, ease of installation).

According to Table 1, "vibrations" can be considered as a possible energy source to produce electricity to operate wireless sensor nodes. Vibrational energy can be captured using a suitable mechanical-to-electrical energy generator that uses electromagnetic, electrostatic, or piezoelectric principles [6]. However, as the majority of vibration energy harvesters are resonant devices that require high frequencies, they cannot be expected to be practical for huge civil infrastructure projects having low natural frequencies.

Figure 1. Charging status of the solar rechargeable batteries of the SHM system on the second Jindo Bridge [2].
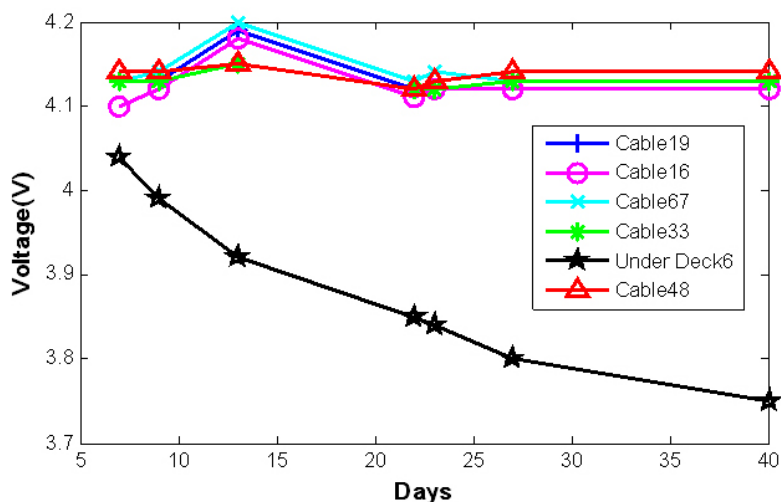
Given that cable-stayed bridges are usually located in windy areas, wind power generation may be a desirable solution for powering a wireless sensor. In recent years, micro-wind turbines have received a considerable amount of attention, and several research groups have demonstrated the effectiveness of small airflow harvesters, as summarized in Table 2 [7]. A comparison of Tables 1 and 2 demonstrates that the power densities of micro-wind turbines are comparable to those of energy-harvesting technologies. However, most studies of micro-wind turbines have mainly focused on the size of the turbine without considering practical implementation issues such as the wind speed, wind direction on the installation site, or the power consumption of an actual wireless sensor node. A practical approach to assist in implementing wireless sensors is still required.

Table 2. Summary of current small-size wind turbines.

| Author	Number of Blades	Rotor Tip Diameter (cm)	Air Speed (m/s)	Maximum Power (mW)	Power Density (mW/cm^2)
Federspiel *et al.* (2003) [8]	4	10	2.5	8	0.10
Priya *et al.* (2007) [9]	12	10.2	4.4	5	0.06
Rancourt *et al.* (2007) [10]	3	4.2	11.8	130	9.38
Xu *et al.* (2009) [7]	4	7.6	4.5	18	0.10

In this study, the applicability of small-size wind-power generators (*i.e.*, micro-wind turbines) for operating a wireless sensor (*i.e.*, Imote2 [11]) under the actual wind conditions at the bridge site was extensively investigated. To this end, the wind environment around the bridge and the power consumption of the Imote2 was examined first. After the available alternators and rotors were carefully selected to make an effective small-size wind generator, a series of experiments was carried out to find the turbine best able to generate the largest amount of power. Finally, to validate its feasibility for powering a wireless sensor experimentally, an actual power charging test is conducted with a horizontal-axis micro-wind turbine having six-blade combined with a wireless sensor.

2. Preliminary Investigations

2.1. Wind Environment at the Bridge Site

Prior to considering the wind turbines, it is necessary to investigate the wind environment around the second Jindo Bridge, which is considered as a test structure, and to find an appropriate location for a wind turbine on the bridge where a PV cell is not applicable. According to records from the Korean Meteorological Administration Center (KMAC) [12], the average wind speed in the Jindo Island area for the last five years has been about 5.3 m/s (see Figure 2).

Figure 2. Wind record in Jindo area from KMAC [12]: (**a**) wind speed record over the last five years; (**b**) wind rose in 2011.

(**a**)

(**b**)
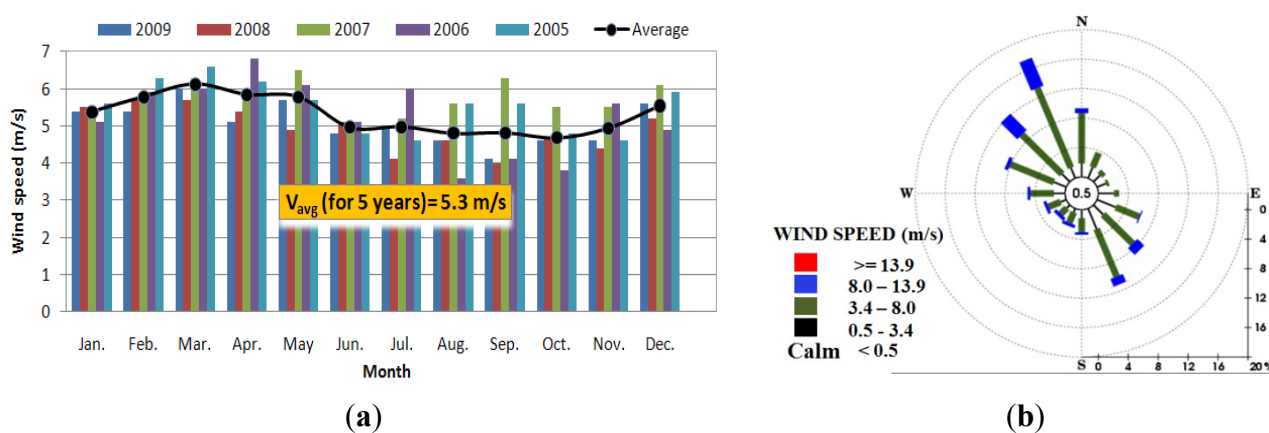
To investigate the actual wind environment on the second Jindo Bridge site, an ultrasonic anemometer (see Figure 3(c)) was installed on the right quarter of the mid-span and the wind distribution was recorded from October, 2011 to April, 2012. From the wind distribution in Figure 3(d), the average wind speed was 4.4 m/s, which is lower than that of the general Jindo area, at 5.3 m/s. In addition, the cut-in speed of the proposed micro wind turbine is 3.5 m/s, which accounts for 50% of the total distribution.

Figures 2(b) and 3(e) show a wind rose diagram in the horizontal direction for the Jindo Bridge site according to the KMAC records and the records from the installed anemometer, respectively. A wind rose is a graph that gives information about how the wind speed and direction are typically distributed at a particular location. Using a polar coordinate system, the frequency of wind over a long time period is plotted according to the wind direction, with color bands showing wind ranges. The directions of the rose with the longest spoke show the wind direction with the greatest frequency. It is clear that the wind direction from the two different records showed similar trends and that the wind mainly blows from the north-west and the south-east, which are perpendicular to the bridge. Figure 3(f) shows a wind rose diagram which graphically presents the vertical wind direction and the corresponding speed measured from the installed anemometer. As shown in the figure, the range of incidence angles is from −10° to 10° with respect to the horizontal axis. In other words, the wind predominantly blows in the horizontal direction.

Figure 3. Wind record measured at the Jindo Bridge: (**a**) overview of the Jindo Bridge; (**b**) anemometer at the bottom of the girder; (**c**) anemometer at the top of the girder; (**d**) wind distribution; (**e**) wind rose in the horizontal direction; (**f**) wind rose in the vertical direction.

(**a**)   (**b**)   (**c**)

(**d**)   (**e**)   (**f**)
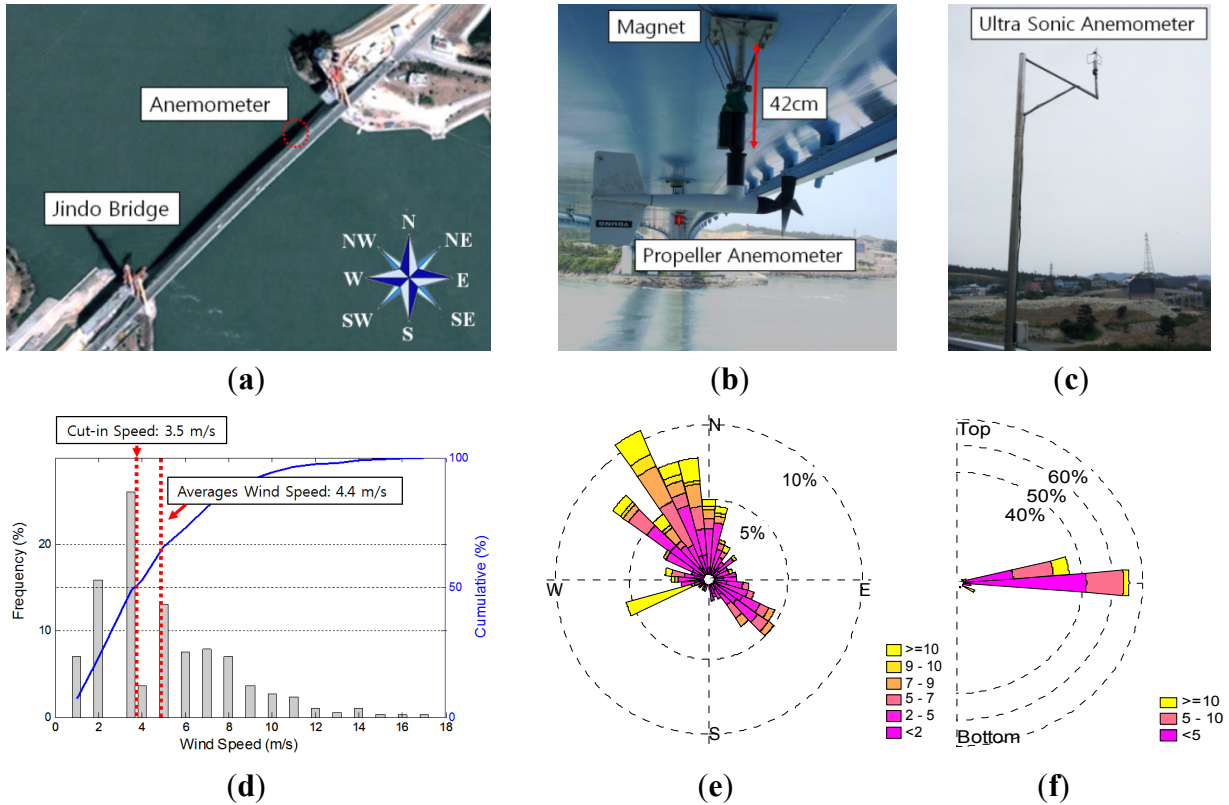
Based on the wind direction data, to find an appropriate location on the girder section for wind energy harvesting, a computational fluid dynamics (CFD) analysis was carried out, as shown in Figure 4. The result shows the wind speed by color ranging from minimum (blue) to maximum (red). As the sensors need to be placed under the girder section, the location with the greatest potential for the proposed wind turbine is the lower edge part of the bridge. This is depicted with the red circle in Figure 4.

Figure 4. CFD analysis result and possible installation location.
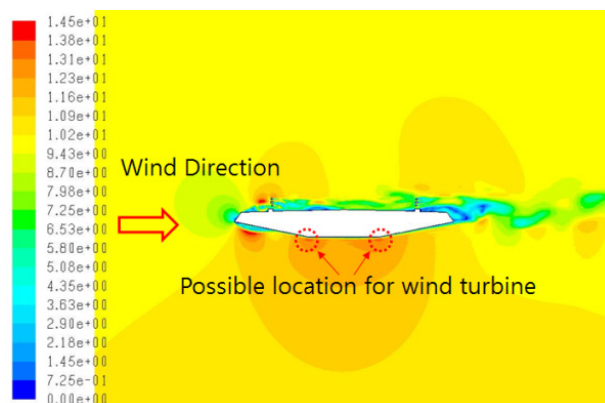
To find the most feasible place under the girder section for the installation of a wind turbine based on the CFD analysis, a propeller-type anemometer (model RM YOUNG 05103V, see Figure 3(b)) was installed on the right quarter of the mid-span, and an ultra-sonic anemometer (model RM YOUNG 81000, see Figure 3(c)) was located at the top of the girder. The propeller-type anemometer was fixed with eight magnets which are capable of holding 10 kg each. If the proposed wind turbine is placed at this location, it can handle airflows of more than 50 m/s with eight magnets.

The wind speed was then measured from 7 a.m. to 12 p.m. on May 25, 2012. Figure 5 plots the ten-minute average wind speed from the top to the bottom of the girder. Taking into account the fact that the mean wind speed of the top of the girder was 1.91 m/s, the wind speed of 2.21 m/s from the bottom of the girder is slightly faster, which supports the CFD test results in Figure 4.

Figure 5. Wind speed measurement data at the bridge site (May 25, 2012).
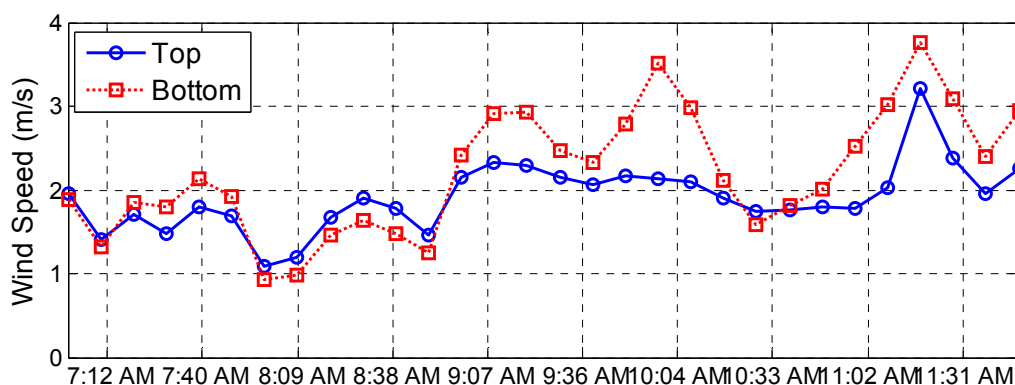

2.2. Power Consumption of a Wireless Sensor Node (*i.e., Imote2*)

The crucial component of the wireless sensor is MEMSIC's Imote2 wireless smart sensor platform, which uses an Intel PXA271 XScale® processor running at 13-416 MHz and an MMX DSP Coprocessor [11]. Imote2's large memory size of 32 MB enables longer measurements, as well as on-board computation. Imote2 is operated with software provided by the Illinois Structural Health Monitoring Project (ISHMP) Services tool suite [13]. The ISHMP tool suite includes numerous useful applications, such as remote sensing, synchronized sensing, an autonomous monitor, and reliable communications.

To investigate its power consumption, the Imote2 was connected to a SHM-A sensor board [14] that employs a tri-axial accelerometer, ST Microelectronic's LIS344ALH, to measure three-axis acceleration data.

The sensing parameter was set to 7500 data points with a sampling rate of 25 Hz, which corresponds to a sensing time of five minutes. This is a sufficient amount of data for capturing the dynamic characteristics of the second Jindo Bridge for one day. Using these parameters, the current draw for each sensing step was measured by supplying constant voltage with a DC power supply.

Figure 6 shows the power consumption during 5 min of sensing. The measured power consumption levels for each sensing step are summarized in Table 3. It was found that a total of 82.66 mWh of energy was required for a one day sensing event.

Figure 6. Power consumption of the wireless sensor.
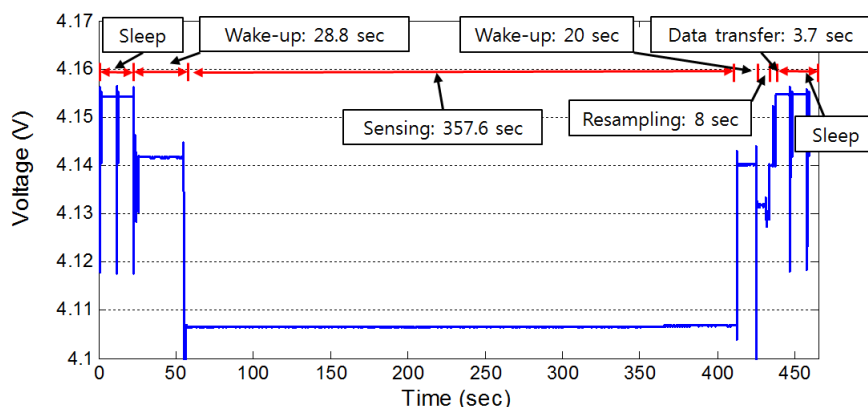
Table 3. Estimated daily power consumption of imote2.

| Mode	Voltage (V)	Current (mA)	Power (mW)	Duration	Power Consumption (mWh)
Wake-up	4.14	47	199	48.8 s	2.7
Sensing	4.11	169	695	357.6 s	69
Resampling	4.13	80	330	8 s	0.73
Data transfer	4.14	55	228	3.7 s	0.23
Sleep	4.15	0.1	0.42	24 h	10
Total					82.66

3. Micro-Wind Turbines

The main components of a typical wind turbine are an alternator and a rotor consisting of blades with aerodynamic surfaces. According to the Betz law, the theoretical maximum power coefficient (C_p) can be as high as 59.26% for an idealized wind turbine. C_p is defined as the ratio of the electrical energy over the kinetic energy of the wind crossing the area swept by the wind turbine. However, in micro wind turbine, due to low efficiency of the generator and the viscous drag of the rotors, the total efficiency is significantly degraded. The major reasons for inefficiency are: (1) relative high viscous drag on the blades at low Reynolds number (*i.e.*, around 100,000), (2) bearing and thermal loss which are significant in a small scale wind turbine and (3) high electromagnetic interferences. The theoretical maximum C_p of the micro wind turbine having a rotor-tip-diameter of less than 10 cm and a direct drive generator without a gearbox are limited to 14.8% [7].

In order to develop an efficient micro-wind turbine, its type (*i.e.*, a horizontal-axis type or a vertical-axis type) was carefully determined. According to a wind rose diagram in the vertical direction on the Jindo Bridge (*i.e.*, Figure 3(f)), the wind predominantly blows in the horizontal direction. From a theoretical point-of-view, a vertical-axis type is the most suitable solution to accept wind from different directions. In this case, however, a horizontal-axis type was chosen due to its higher efficiency.

On the other hand, based on a wind rose diagram in the horizontal direction (*i.e.*, Figure 3(e)), the wind has different azimuths with time, so a tail fin was incorporated into a horizontal-axis micro-wind turbine for aligning a rotor with the oncoming wind as shown in Figure 7(a). Note that if the blowing wind has varying incidence angles with time, a countermeasure should be considered because of the different interaction effect between the wind with varying incidence angles and a structure.

Figure 7. Horizontal-axis wind turbine: (**a**) side view of the wind turbine; (**b**) two-blade propeller; (**c**) three-blade propeller; (**d**) six-blade propeller.

(**a**)

(**b**)

(**c**)

(**d**)
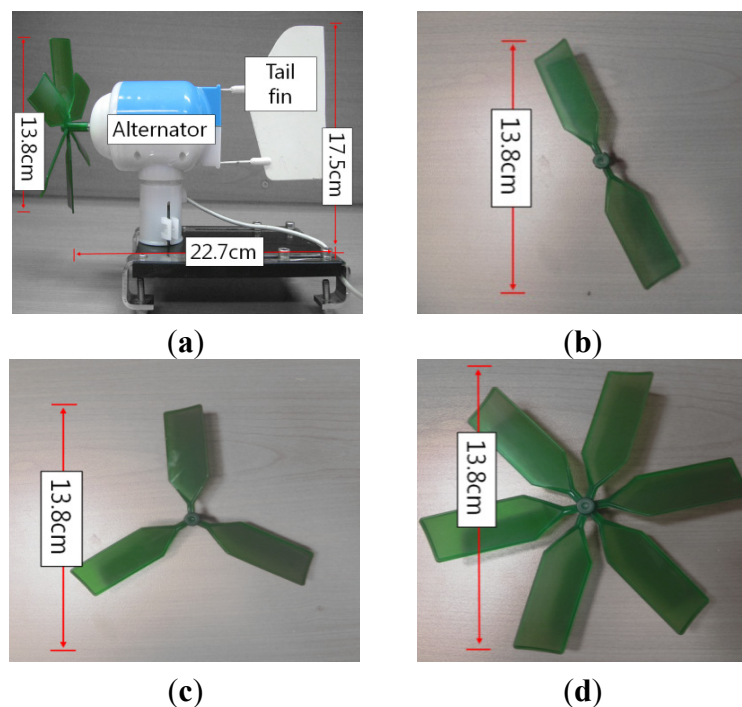
In a wind turbine, an alternator is a very important electrical part and contains all the coils of wire that will have voltage induced as the magnets of the rotor pass over them. In this study, a three-phase brushless alternator manufactured by Hankuk Relay (model HR-W35V [15]) is used as the generator to produce power from the airflow. Its electric characteristics are summarized in Table 4. A brushless alternator has several advantages over the brushed type, including higher efficiency and reliability, reduced noise, a longer lifetime (no brush erosion), and more power. Also, a three-phase alternator is known to be typically 150% more efficient than a single-phase alternator in the same power range.

Table 4. Electric characteristics of the alternator.

Alternator	Type	Phase Resistance (Ω)	Conversion Coefficient K (V/rad/s)
HR-W35V	3-Phase	70	1.26×10^{-1}

Another important part of a wind turbine is the rotor. The horizontal-axis rotor, which is known to be the most efficient, was tested, as depicted in Figure 7(a). Various small rotors were investigated to maximize the performance of the turbine, and three rotors with diameters of 13.8 cm, as shown in Figures 7(b–d), were selected. The selected rotors were taken from a 'Green Science windmill generator kit'.
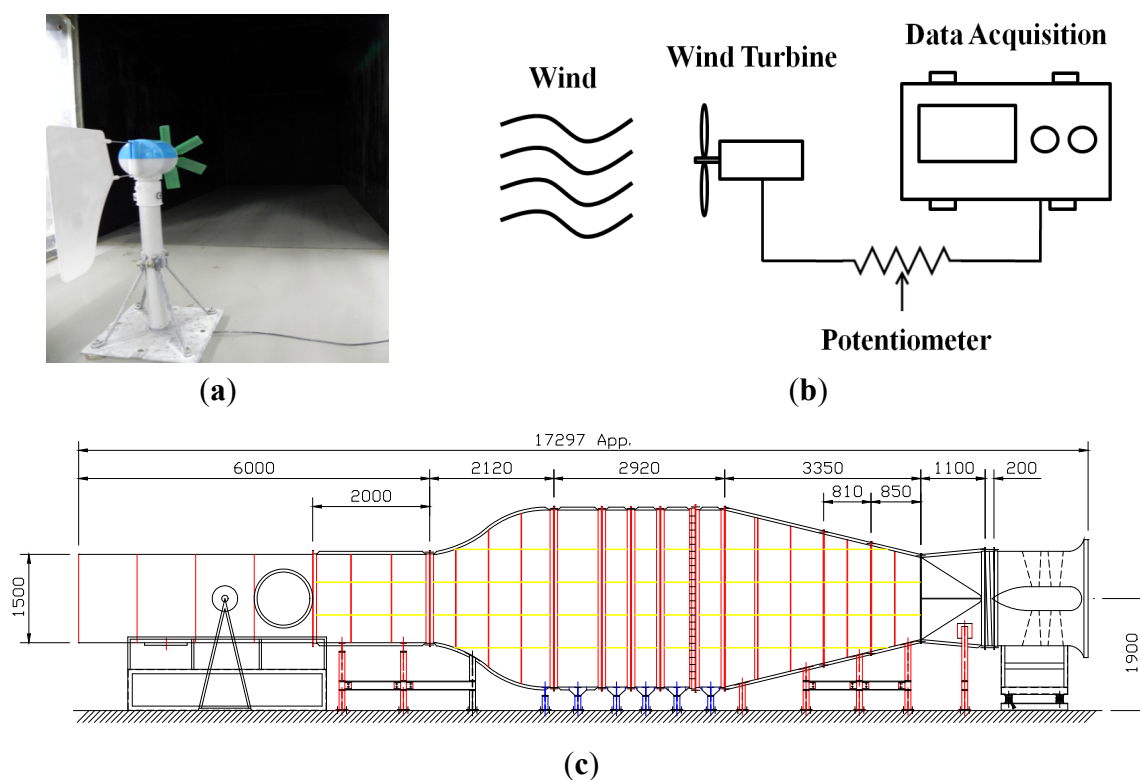
4. Performance Test

4.1. Experimental Setup

To verify the performance of the three micro-wind turbines (*i.e.*, the three horizontal-axis turbines in Figure 7), a series of the experimental tests was carried out in the wind tunnel with a constant wind

speed. The dimensions of the wind tunnel used in this test are shown in Figure 8(c). The power generated from the wind turbines passed through a potentiometer varying from 30 Ω to 5 kΩ that was used to tune the resistive loads; at each step, the output voltage from the wind turbines was measured by an oscilloscope, as shown in Figure 8. The weather conditions for the ambient pressure, ambient temperature, and relative humidity in the laboratory were 995.5 hPa, 23 °C and 52%, respectively. Therefore, the air density was 1.1646 kg/m^3.

Figure 8. Experimental setup: (**a**) wind turbine in the wind tunnel; (**b**) configuration of the experiment; (**c**) wind tunnel facility.

(**a**)   (**b**)

(**c**)

4.2. Experimental Results

The first experiment was done to evaluate the performance of the three different wind turbines under the same wind environment with an RMS wind speed of 7 m/s. The RPM (revolutions per minute) of the wind turbines was adjusted as the resistance of the potentiometer varied under the same wind environment and the output voltage at each load resistance step was measured.

Figure 9 shows the RPM of the rotor *versus* the output power with the three different types of rotors. Under the same wind speed, the RPM *versus* the generated power for three-blade shapes are plotted by adjusting the resistance to find the maximum output power. From the result, it was demonstrated that the wind turbine with six-blade rotor had the most powerful performance, having a generated power of 439 mW with a wind speed of 7 m/s. In terms of the power density shown in Table 5, the case with six blades also showed a maximum of 2.93 mW/cm^2, while the case with three showed 1.69 mW/cm^2 and that with two blades showed 1.17 mW/cm^2.

Figure 9. Wind turbine efficiencies for three different types of rotors (at 7 m/s).
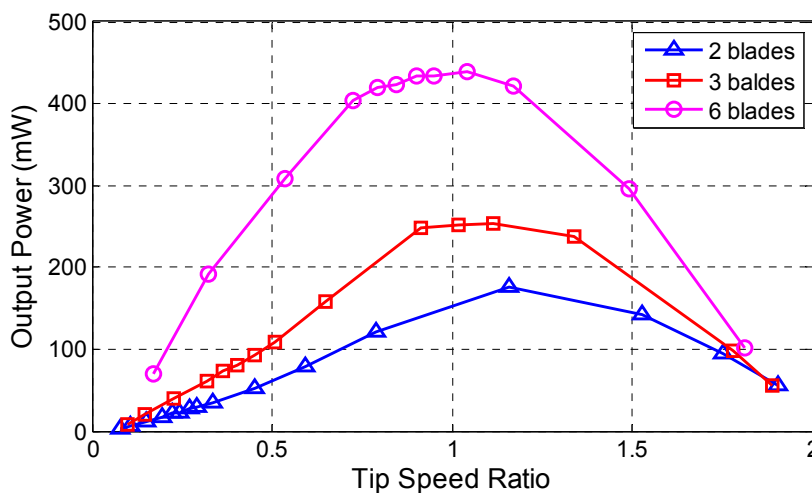

Table 5. Output power with different type of rotors.

Rotor type	Diameter (cm)	Maximum Output (mW)	Power Density (mW/cm^2)
Two blades	13.8	175.05	1.17
Three blades	13.8	252.80	1.69
Six blades	13.8	438.79	2.93

Next the performances under different wind speeds ranging from 3.5 m/s to 7 m/s were explored for the best performing six-blade rotor. Figure 10 shows the evolution of the overall generated power of the wind turbine for five different wind speeds (*i.e.*, 3.5 m/s, 4 m/s, 5 m/s, 6 m/s and 7 m/s). For a wind speed of 3.5 m/s, which is the cut-in wind speed of the proposed wind turbine, a maximum of 28.88 mW power was achieved and a maximum power of 438.79 W at a wind speed of 7 m/s was obtained. The output voltage measurements at each maximum power point are summarized in Table 6.

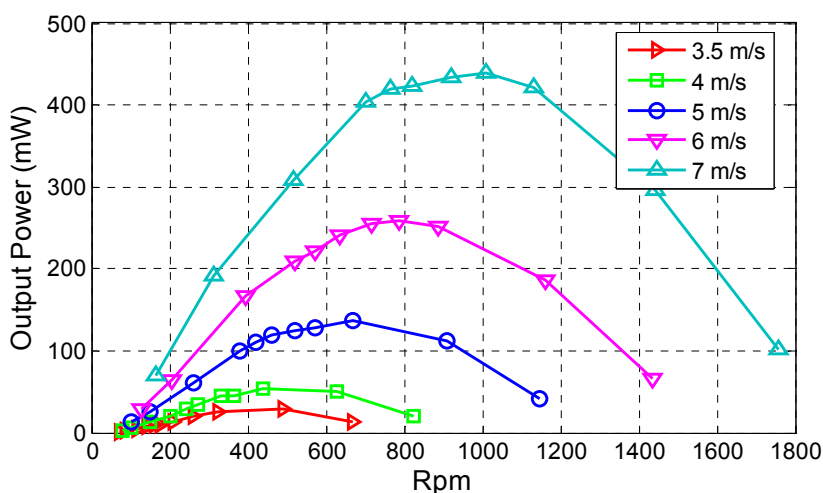**Figure 10.** Overall generated power of a micro-wind turbine with a six-blade rotor.

Table 6. Outputs at the maximum power points.

Wind Speed (m/s)	Voltage (V)	Current (mA)	Power (mW)
3.5	5.73	5.04	28.88
4	5.06	10.54	53.30
5	8.09	16.85	136.34
6	9.66	26.84	259.32
7	12.57	34.91	438.79

4.3. Validation of Self-Sufficient Operation Capacity

To test the feasibility of charging through the proposed wind turbine, it was connected to a rechargeable battery and a charging circuit as shown in Figure 11. The main component of the charging circuit is a buck regulator (model LM2596). The LM2596 is a high-efficiency buck regulator that supports an input range of 7 V~30 V and an adjustable output range of 1.25 V~35 V. The output voltage of the LM2596 was set to 4.2 V to charge a Li-polymer rechargeable battery having a nominal voltage of 3.7 V, and a 230-mAh Li-polymer rechargeable battery was used.

**Figure 11.** Charging system for the wireless sensor (Imote2).
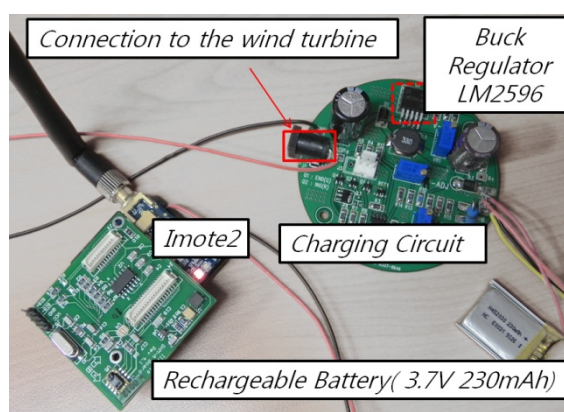
The actual charging and sensing test was carried out with the same sensing parameters as done in Table 3. The total power consumption during the test was 72.66 mWh as the power loss during the sleep mode (*i.e.*, 10 mWh) was excluded from the power consumption for one day in Table 3.

In order to check the time required to recover the power loss during sensing, the wireless sensor node was equipped with the wind turbine and the charging circuit. Its result (*i.e.*, the "with charging" case) was compared with that of a sensor node without the turbine and the circuit (*i.e.*, the "without charging" case). Due to the limitation of the regulator and the impedance mismatch between the wind turbine and the charging circuit [16], wind speeds lower than 7 m/s could not be used for the charging test.

Figure 12 shows the battery voltage variations of two cases (*i.e.*, the "with charging" and the "without charging" cases) at a wind speed of 7 m/s. As shown in the figure, battery voltages in both cases declined rapidly during sensing due to the high level of power consumption. After sensing, the battery level in the "without charging" case had decreased, though it slightly recovered (*i.e.*, from 4.05 V to 3.95 V), showing a voltage drop of 0.1 V. In the 'with charging' case, the battery level

during the sensing process showed a slight decrease; however, with charging from the wind turbine, the degree of the decline was more moderate, and showed a steadily increasing trend in terms of the battery level requiring a recovery time of 33 min.

Figure 12. Battery levels according to the charging condition.
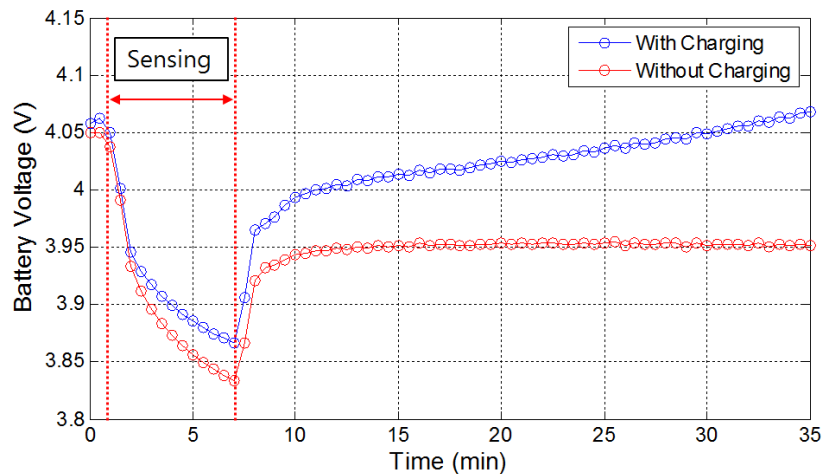
It was found from the actual power-charging test that the maximum power at 7 m/s (*i.e.*, 438.79 mW) was not extracted due to the impedance mismatch between the wind turbine and the charging circuit. The output voltage at the maximum power was 12.57 V, as shown in Table 6; however, the voltage during the charging test from the charging circuit was 4.99 V. Under this impedance condition, the RPM was 435 rad/s and the corresponding generated output was 265 mW, as shown in Figure 13.

Figure 13. Output power and output voltage (at 7 m/s): (**a**) RPM *versus* the output voltage; (**b**) RPM *versus* the output power.

(**a**)   (**b**)
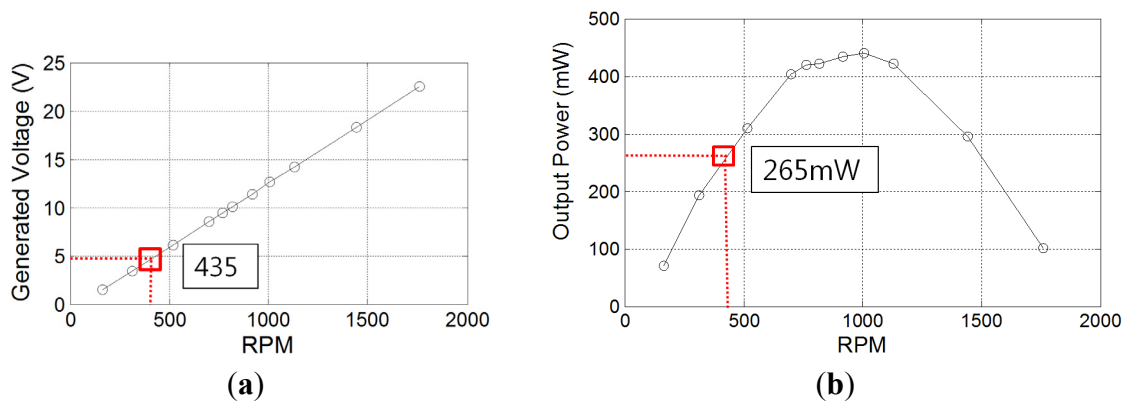
Theoretically, 16.4 min is required to compensate for the power consumption of 72.66 mWh during the test (*i.e.*, 72.66 mWh/265 mW = 16.4 min). In practice, however, it took 33 min to recover the power loss completely. Therefore, the charging efficiency to the battery in this case was determined to be about 50%. If the maximum peak power [16] can be extracted and the charging efficiency to battery is taken into account, it would take 19.8 min to recover the power loss. The maximum power can be harvested continuously through maximum power point tracking (MPPT) technique [16–18] that tracks the peak power points of the power generating system for any given environmental conditions.

The charging time under different wind speeds was estimated and is summarized in Table 7. Here, the charging efficiency to the battery for all the different wind speed cases is assumed to be identical, because the parameters affecting the charging efficiency, such as the charging method and the battery status, are almost the same for the different wind speeds. As seen from the table, there are large variations in the recovery time depending on the wind speed. At a wind speed of 7 m/s, only a short duration of wind of 19.8 min can operate the sensing process for a day, whereas 63.9 min and 163.4 min are required at a wind speed of 5 m/s and 4 m/s, respectively. It was found that a strong wind with a short duration was more efficient than a long-lasting low wind flow. Since the average wind speed at the Jindo Bridge site is 4.4 m/s and the cumulative wind distribution at 4 m/s is more than 50% (see Figure 3(d)), wind blowing at 4 m/s or higher wind speed for 163.4 min (*i.e.*, about 2.7 h) is not a rare case. Moreover, the electricity generation process does not need to be continuous in this case. Even though the electricity is generated intermittently from the turbine, sufficient electrical energy can be ensured as long as the total electricity generation period is about 2.7 h in the case of 4 m/s or higher wind speed. This is quite feasible based on the wind measurement data from the Jindo Bridge site. Therefore, a wireless sensor with the proposed micro-wind turbine installed under the deck of the bridge may successfully perform the sensing process in most cases. However, if the proposed micro-wind turbine cannot provide the sufficient electricity for a stable functioning of the wireless sensor due to lacks of wind and electricity generation period for several consecutive low-wind days, combining a shadowed solar panel with the proposed wind turbine can be another alternative.

The efficiency of the proposed wind turbine varies from 7.50% to 14.25% for corresponding wind speeds of 3.5 m/s to 7 m/s as seen from Table 7. This large amount of variation may result from friction in the generator, internal electrical resistance and efficiency of the rotors.

Table 7. Estimated charging time.

Wind Speed (m/s)	Maximum Measured Power (mW) [A]	Recovery Time at Measured Power (min)	Available Wind Power (mW) [B]	Efficiency * (%)
3.5	28.88	301.5	384.77	7.50
4	53.30	163.4	574.35	9.28
5	136.34	63.9	1121.78	12.15
6	259.32	33.6	1938.44	13.38
7	438.79	19.8	3078.18	14.25

* Efficiency (%) = A/B * 100.

5. Conclusions

In this paper, the feasibility of using micro-wind turbines to power wireless smart sensors on a cable-stayed bridge was investigated. To this end, both the wind environment of the possible installation location at an in-service cable-stayed bridge (*i.e.*, the second Jindo Bridge in Korea) and the power consumption of a wireless sensor node (*i.e.*, Imote2) were carefully examined.

In order to develop an effective small-size wind turbine, possible alternators and rotors were examined. For the experimental tests, three specially designed micro-wind turbines were considered: horizontal-axis turbines having two, three and six blades, respectively. To determine the wind turbine which performs best, a series of the experimental tests was conducted in which the output voltages of

the turbines were compared under five different wind speeds ranging from 3.5 m/s to 7 m/s. It was found that the horizontal-axis wind turbine having six blades offered the highest level of performance.

To verify its actual power-charging capability, an additional test was carried out with the combination of a horizontal-axis six-blade wind turbine, a wireless sensor node and a charging circuit. It was observed from the test at a wind speed of 7 m/s that the wireless sensor with the wind turbine showed an increasing voltage status and completely recovered the power loss within 33 min. On the other hand, the sensor node without a power-charging system drained the energy by 0.1 V. From the test results, the actual charging time for one day sensing event is calculated under the assumption that maximum output powers at corresponding wind speeds are extracted. According to the estimated charging time, it is expected that a wireless sensor with the proposed micro-wind turbine can successfully perform the sensing process at the Jindo Bridge site when there exists a wind flow of 4 m/s or higher for about 2.7 h a day. This is quite feasible based on the wind measurement data from the bridge site. Therefore, it is concluded that the micro-wind turbine can generate sufficient electricity for powering a wireless sensor under moderate wind conditions. If the proposed micro-wind turbine cannot generate the sufficient electricity due to lack of electricity generation period for several consecutive low-wind days, combining the proposed turbine with a shadowed solar panel can be another alternative.

A further step of the research is to design an elaborate charging circuit with the maximum peak power tracking and the use of super capacitors as storage devices for fast charging. And then, the long-term performance of the wind turbine combined with Imote2 on the bridge will be investigated.

Acknowledgement

References

1. Cho, S.; Jo, H.; Jang, S.; Park, J.; Jung, H.J.; Yun, C.B.; Spencer, B.; Seo, J.W. Structural health monitoring of a cable-stayed bridge using wireless smart sensor technology: Data analyses. *Smart Struct. Syst.* **2010**, *6*, 461–480.
2. Jang, S.; Jo, H.; Cho, S.; Mechitov, K.; Rice, J.A.; Sim, S.H.; Jung, H.J.; Yun, C.B.; Spencer, B.F., Jr.; Agha, G. Structural health monitoring of a cable-stayed bridge using smart sensor technology: Deployment and evaluation. *Smart Struct. Syst.* **2010**, *6*, 439–459.
3. Mathúna, C.Ó.; O'Donnell, T.; Martinez-Catala, R.V.; Rohan, J.; O'Flynn, B. Energy scavenging for long-term deployable wireless sensor networks. *Talanta* **2008**, *75*, 613–623.
4. Miller, T.I.; Spencer, B.F., Jr.; Li, J.; Jo, H. *Solar Energy Harvesting and Software Enhancements for Autonomous Wireless Smart Sensor Networks*; NSEL Report NO. NSEL-022 2010; Urbana and Champaign, IL, USA, 2010.

5. Raghunathan, V.; Kansal, A.; Hsu, J.; Friedman, J.; Srivastava, M. Design Considerations for Solar Energy Harvesting Wireless Embedded Systems. In *Proceedings of the Fourth International Symposium on Information Processing in Sensor Networks*, Los Angeles, CA, USA, 25–27 April 2005.

6. Beeby, S.; Tudor, M.; White, N. Energy harvesting vibration sources for microsystems applications. *Meas. Sci. Technol.* **2006**, *17*, 175–195.

7. Xu, F.; Yuan, F.; Hu, J.; Qiu, Y. Design of a Miniature Wind Turbine for Powering Wireless Sensors. In *Proceedings of the SPIE Annual Symposium on Smart Structures and Materials and Nondestructive Evaluation and Health Monitoring*, San Diego, CA, USA, 7–11 March 2010.

8. Federspiel, C.C.; Chen, J. Air-Powered Sensor. In *Proceedings of the IEEE Sensors 2003 Conference*, Toronto, Canada, 22–24 October 2003.

9. Priya, S.; Chen, C.T.; Fye, D.; Zahnd, J. Piezoelectric windmill: A novel solution to remote sensing. *Jpn. J. Appl. Phys.* **2005**, *44*, 104–107.

10. Rancourt, D.; Tabesh, A.; Fréchette, L.G. Evaluation of Centimeter-Scale Micro Windmills: Aerodynamics and Electromagnetic Power Generation. In *Proceedings of the Technical Digest PowerMEMS 2007*, Freiburg, Germany, 27–29 November 2007.

11. Crossbow Technology, Inc. Imote2 Hardware Reference Manual. Available online: http://www.xbow.com.cn/LinkClick.aspx?fileticket=i7FK6%2B1oodU%3D&tabid=121 (accessed on 29 February 2012).

12. Korean Meteorological Administration Center (KMAC). Past Wind Records on Jindo Areas. Available online: http://jindo.kma.go.kr/ (accessed on 29 February 2012).

13. Illinois Structural Health Monitoring Project. Available online: http://shm.cs.uiuc.edu/ (accessed on 12 March 2012).

14. Rice, J.A.; Mechitov, K.; Sim, S.H.; Nagayama, T.; Jang, S.; Kim, R.; Spencer, B.F., Jr.; Agha, G.; Fujino, Y. Flexible smart sensor framework for autonomous structural health monitoring. *Smart Struct. Syst.* **2010**, *6*, 423–438.

15. Hankuk Relay Co. Ltd. Available online: http://www.hankukrelay.co.kr/ (accessed on 29 February 2012).

16. Park, C.; Chou P.H. AmbiMax: Autonomous Energy Harvesting Platform for Multi-Supply Wireless Sensor Nodes. In *Proceedings of the 3rd Annual IEEE Communications Society Conference on Sensor, Mesh and Ad Hoc Communications and Networks (SECON 2006)*, Reston, VA, USA, 25–28 September 2006.

17. Tan, Y.K.; Panda, S.K. Self-autonomous wireless sensor nodes with wind energy harvesting for remote sensing of wind-driven wildfire spread. *IEEE Trans. Instrum. Meas.* **2011**, *60*, 1367–1377.

18. Tan, Y.K. Optimized wind energy harvesting system using resistance emulator and active rectifier for wireless sensor nodes. *IEEE Trans. Power Electron.* **2011**, *26*, 38–50.